LBL-12863
Preprint c.2

Lawrence Berkeley Laboratory

UNIVERSITY OF CALIFORNIA

RECEIVED
LAWRENCE
BERKELEY LABORATORY

OCT 21 1981

LIBRARY AND
DOCUMENTS SECTION

Materials & Molecular Research Division

Submitted to the Journal of Aerosol Science

NONCIRCULAR COLLISION CROSS SECTIONS OF INDUCED ELECTRIC DIPOLES

Joseph C. Farmer

September 1981

TWO-WEEK LOAN COPY

This is a Library Circulating Copy which may be borrowed for two weeks. For a personal retention copy, call Tech. Info. Division, Ext. 6782

LBL-12863 c.2

Prepared for the U.S. Department of Energy under Contract W-7405-ENG-48

DISCLAIMER

This document was prepared as an account of work sponsored by the United States Government. While this document is believed to contain correct information, neither the United States Government nor any agency thereof, nor the Regents of the University of California, nor any of their employees, makes any warranty, express or implied, or assumes any legal responsibility for the accuracy, completeness, or usefulness of any information, apparatus, product, or process disclosed, or represents that its use would not infringe privately owned rights. Reference herein to any specific commercial product, process, or service by its trade name, trademark, manufacturer, or otherwise, does not necessarily constitute or imply its endorsement, recommendation, or favoring by the United States Government or any agency thereof, or the Regents of the University of California. The views and opinions of authors expressed herein do not necessarily state or reflect those of the United States Government or any agency thereof or the Regents of the University of California.

NONCIRCULAR COLLISION CROSS SECTIONS OF INDUCED ELECTRIC DIPOLES

Joseph C. Farmer

Materials and Molecular Research Division,
Lawrence Berkeley Laboratory, and Department of Chemical Engineering,
University of California Berkeley, Berkeley CA 94720

ABSTRACT

Highly noncircular cross sections for two capture regimes, flowline interception and inertial capture, are computed from three-dimensional trajectory calculations thereby allowing for asymmetry. Calculations of the collision efficiencies and cross sections between pairs of induced electric dipoles available in the literature are incorrect for electric field orientations perpendicular to the direction of particle travel because particle motion about the collector was inadvertently assumed to be symmetric about the axis of approach. These circular collision cross sections were deduced from two-dimensional trajectories and can lead to collision efficiency predictions which are too large by a factor of 3.

This work was supported by the Director, Office of Energy Research, Office of Basic Energy Sciences, Materials Sciences Division of the U.S. Department of Energy under Contract No. W-7405-ENG-48.

NOMENCLATURE

Noncapitalized Symbols

a_c critical radius for circular collision cross section (m)

$\vec{f}_e$ electric dipole-dipole force vector

g_c gravitational constant ($Kg \cdot m \cdot s^{-2}/N$)

$\vec{g}$ acceleration of gravity vector $(9.81)(m \cdot s^{-2})$

r radial coordinate in spherical system (m)

$\vec{r}$ positional vector (m)

r_i radial separation of individual poles of collector and particle for i = 1 through 4 (m)

t time(s)

z coordinate of small particle's position parallel to flow with collector's center taken as the origin (m)

y coordinate of small particle's position parallel to electric field (perpendicular orientation case) with collector's center taken as origin (m)

x coordinate orthogonal to both z and y (m)

Capitalized Symbols

E_c fractional collision efficiency

F_d viscous drag force on sphere (N)

$\vec{F}_e$ Electric dipole-dipole force vector (N)

F_r r-component of $\vec{F}_e$ (N)

F_θ θ-component of $\vec{F}_e$ (N)

F_z z-component of $\vec{F}_e$ (N)

F_y y-component of $\vec{F}_e$ (N)

$\vec{M}$ electric dipole moment of polarized sphere (C·m)

$\vec{M}_c$ $\vec{M}$ for collector (C·m)

$\vec{M}_p$ $\vec{M}$ for smaller particle (C·m)

R radius of spherical particle (m)

R_c R for collector (m)

R_p R for smaller particle (m)

$\vec{S}$ velocity vector of smaller particle entrained in collector's flow field ($m \cdot s^{-1}$)

$\vec{U}$ velocity vector of gas moving past collector ($m \cdot s^{-1}$)

U_∞ free-stream magnitude of $\vec{U}$ ($m \cdot s^{-1}$)

W_{pc} work stored between two dipoles "p" and "c" when held at a distance "r" and angle "θ" relative to one another (J)

Dimensionless Parameters

K_v a parameter in trajectory equations determining the length of the time scale for a collision

K_f a parameter in trajectory equations describing the magnitude of the ratio of the viscous force to the inertial force

K_e a parameter in trajectory equations describing the magnitude of the ratio of the dipole-dipole force to the inertial force

Greek Symbols

ε_p dielectic constant of particle and collector

ε_o permittivity of free space $(8.854 \times 10^{-12})(F \cdot m^{-1})$

ρ gas density $(kg \cdot m^{-3})$

ρ_p particle and collector density $(kg \cdot m^{-3})$

μ gas viscosity $(kg \cdot m^{-1} \cdot s^{-1})$

θ angular coordinate in spherical system

ω angular frequency or time normalization constant (s^{-1})

Other Symbols

* as a superscript denotes nondimensionalized variables or operators

$\perp$ denotes orientation of the electric field perpendicular to the direction of particle motion

// denotes orientation of the electric field parallel to the direction of particle motion

INTRODUCTION

The objective of this study is to correctly determine aerodynamic collision cross sections and corresponding collision efficiencies between pairs of spherical particles polarized by an external electric field for the case where flow and electric fields are perpendicular and particle motion symmetric about the axis of approach cannot be assumed. Previously, such cross sections have been incorrectly assumed circular and deduced from two-dimensional trajectories by symmetry arguments (Semonin, 1963, 1965).

This work is significant in that it shows collision cross sections between pairs of induced dipoles to be highly noncircular when flow and electric field orientations are perpendicular. In such cases, three-dimensional trajectories must be used to deduce the collision cross sections and corresponding collision efficiencies. Furthermore, it is shown that collision efficiencies determined from circular cross sections lead to significant qualitative and quantitative errors in this instance.

BACKGROUND

Knowledge of the aerodynamic collision cross section between pairs of small particles is important in calculating efficiencies of mist and dust collection equipment such as spray scrubbers (Nielsen, 1976) and acoustic agglomerators (Shaw, 1979), and is central to understanding droplet growth mechanisms in clouds (Sartor, 1960). In principle, collision efficiencies can be enhanced by using external electric fields to induce dipole moments in particles, thereby extending the distance of interaction between collision partners. For specific orientations of

the electric field with respect to the direction of particle motion, a net attraction results.

Collisions occur between particles of different sizes in scrubbers due to their different terminal velocities or in acoustic agglomerators due to their difference in relative entrainment in the oscillatory flow of the acoustic wave. The larger of the two particles is usually referred to as the collector.

To determine collision efficiencies from first principles requires that a series of particle trajectories around the collector be calculated taking into account deflection of the smaller particle by the collector's local flow and electric fields. From grazing particle trajectories the area of the collision cross section, hence the aerodynamic collision efficiency, can be computed as seen by an observer upstream of the collector.

The motion of the small particle about the collector is symmetric about the axis of approach only if all forces acting on the small particle are also axisymmetric respective to the same axis. In this particular case, the collision cross section is appropriately determined from arguments of symmetry by trajectory calculations in only two dimensions. Once the critical radius a_c is found, the area of the collision cross section is taken as πa_c^2 and the fractional collision efficiency, E_c, calculated as

$$E_c = \frac{a_c^2}{(R_p + R_c)^2}$$

where R_p and R_c are the radii of the particle and collector, respectively (See Fig. 1). For two induced dipoles undergoing aerodynamic collision,

the assumption of symmetric motion is valid for electric field orientations parallel to flow (direction of particle motion).

However, if all forces acting on the particle are not axisymmetric with respect to the axis of approach, determination of the collision cross section from two-dimensional trajectory calculations is not justifiable. This is the case for induced electric dipoles with the external electric field perpendicular to the direction of particle motion. In this instance, one would expect intuitively that trajectories in the plane normal to the dipole moment would suffer a net repulsion whereas trajectories in the plane of the dipole moment, parallel to flow, would experience a strong attraction as the poles of the collector and particle of opposite polarity approach one another. (See Fig. 2). Such asymmetry, as shown in this work, gives rise to highly noncircular collision cross sections which can be determined only from three-dimensional trajectory calculations. These results have not been reported previously in the literature. Below, the definition of the aerodynamic collision efficiency is generalized for noncircularity

$$E_c = \frac{\text{Area of Collision Cross Section}}{\pi(R_p + R_c)^2} \tag{1.b}$$

Semonin and coworkers (1963, 1965) have calculated cross sections and collision efficiencies for pairs of induced electric dipoles for general orientations of the flow and electric fields, including the perpendicular case. However, they inadvertently assumed symmetry and circular collision cross sections in all their calculations. For the reasons discussed above, such assumptions are incorrect except for the parallel orientation of the electric field relative to flow and can lead to significant

qualitative and quantitative errors when estimating collision efficiencies.

In this paper, collision cross sections for pairs of induced dipoles are presented for a spherical neutral collector about 20μ in diameter colliding at terminal velocity with either an 8 or 2μ particle; these interception parameters (R_p/R_c) of 0.4 and 0.1 represent inertial capture and flowline interception regimes, respectively. Calculations for both regimes were done with electric field strengths ranging from 0 to approximately 100 kV/m. Both series of calculations were done for perpendicular and parallel orientations of flow and electric fields for purposes of comparison.

The trajectory equations used assume Stoke's flow around the collector, Stoke's law for deflection of the smaller particle by the collector's flow field, and that both particles are ideal dipoles. Relevant hydrodynamic equations are (Bird, 1960)

$$U_r = U_\infty(1-3/2\ R/r + 1/2\ R^3/r^3)\cos\theta \tag{2.a}$$

$$-U_\theta = U_\infty(1-3/4\ R/r - 1/4\ R^3/r^3)\sin\theta \tag{2.b}$$

$$F_d = 6\pi\mu R U_\infty \tag{3}$$

If particles move only under the influence of gravity, the free-stream velocity used is the terminal velocity

$$U_\infty = \frac{2g\ \rho_p R^2}{9\mu} \tag{4}$$

In these equations U_r and U_θ are the radial and angular velocity components; U_∞ the free-stream velocity; F_d the drag force; R and ρ_p the radius and density of the particle, respectively; μ the gas viscosity; and g the acceleration of gravity.

The electric field surrounding a single conducting sphere in a uniform external electric field is found from a solution of Laplace's equation in spherical coordinates to consist of two components, one due to the external field and the other due to the polarization of the sphere (Corson, 1962). The electric field contribution of the second term is identical to that of an ideal dipole of moment

$$\vec{M} = 4\pi \varepsilon_o \vec{E} R^3 \tag{5}$$

when observed at great distances. Hence, the polarized sphere is said to have a dipole moment of $\vec{M}$ induced by the field $\vec{E}$; ε_o is the permittivity of free space. For a dielectric sphere

$$\vec{M} = \left(\frac{\varepsilon_p - 1}{\varepsilon_p + 2}\right) 4\pi \varepsilon_o \vec{E} R^3 \tag{6}$$

where ε_p is the dielectric constant of the sphere. Since values of ε_p are usually much greater than unity, particles can often be regarded as conducting spheres.

The force of interaction between two induced dipoles is then classically computed as the gradient of the work stored in the system of charges when held in proximity to one another. The work stored between induced (parallel) dipoles "p" and "c" is given in Jackson (1975) as

$$W_{pc} = \frac{|\vec{M}_p| \; |\vec{M}_c|}{r^3} (1 - 3\cos^2\theta) \tag{7}$$

It follows that

$$F_e = -\nabla W_{pc} \tag{8.a}$$

$$F_r = \frac{|\vec{M}_p| \; |\vec{M}_c|}{r^4} (1-3 \cos^2\theta) \tag{8.b}$$

$$-F_\theta = \frac{|\vec{M}_p| \; |\vec{M}_c|}{r^4} (6 \sin\theta \cos\theta) \tag{8.c}$$

These equations for the electric dipole force are valid only at large values of r (r>>R). The most obvious shortcoming of this common model is that even when two dipoles "touch" pole-to-pole the force remains finite, yet one would expect the force to become infinite since the attractive forces are due to interactions between induced <u>surface</u> charges. However, this model is advantageous from the standpoint of its simplicity and ease of evaluation when incorporated into numerical trajectory calculations.

More rigorous equations for the dipole interaction between polarized spheres have been developed by Davis (1964) which are based on a solution of Laplace's equation in bispherical coordinates. These equations have the facility to incorporate net charge and ion image effects into the interaction force. They have been used by Semonin and coworkers in two-dimensional trajectory calculations and are applicable for small distances of separation (1965). However, these equations are tremendously complicated since both the expression for F_r and F_θ involve evaluation of infinite series whose terms are also complicated. In an earlier work Semonin and coworkers (1963) performed similar two-dimensional trajectory calculations using equation 5 and equations 8.b and 8.c. The principal difference in the results obtained is that for a given electric field strength the

collision cross section obtained appears larger when using the more exact equations, probably due to the fact that the exact equations take into account the significantly greater force of interaction when the surfaces of the particles are brought close together. Qualitatively, the results are similar.

Since the electric force of interaction is to be used in a time-consuming computer program it is important from a practical viewpoint to keep expressions as simple, yet as descriptive, as possible. Each iteration involves the simultaneous integration of four to six nonlinear first order ordinary differential equations (for two or three dimensional trajectory calculations) and each integration step requires evaluation of the terms F_r and F_θ. Thus there is incentive to find a reasonable compromise between the more rigorous equations for F_r and F_θ and equations 8.b and 8.c. A suitable pair of approximations should give values approaching those from 8.b and 8.c for large separations and should have forces of attraction approaching infinity when the poles "touch".

A reasonable approximation is to compute the sum of forces acting between individual poles of the two spheres, calculating the polar surface charges from the magnitude of the dipole moments and the sphere diameters. The resulting equations satisfy the above criteria and are summarized below for the x = o plane; generalization for three-dimensions was done through straight forward trigonometric manipulations in the computer algorithm (Farmer, 1981).

$$F_z = \frac{1}{4\pi\varepsilon_o} \frac{|\vec{M}_p|\ |\vec{M}_c|}{R_p R_c} \frac{z}{4} \left(\frac{1}{r_1^{\,3}} - \frac{1}{r_2^{\,3}} - \frac{1}{r_3^{\,3}} + \frac{1}{r_4^{\,3}} \right) \tag{9.a}$$

$$F_y = \frac{1}{4\pi\varepsilon_o} \frac{|\vec{M}_p|\ |\vec{M}_c|}{R_p R_c} \frac{1}{4} \left(\frac{Y_1}{r_1^{\,3}} - \frac{Y_2}{r_2^{\,3}} - \frac{Y_3}{r_3^{\,3}} + \frac{Y_4}{r_4^{\,3}} \right) \tag{9.b}$$

$$y_1 = y + R_p - R_c \qquad r_1 = (z^2 + y_1^2)^{1/2} \tag{9.c\&d}$$

$$y_2 = y + R_p + R_c \qquad r_2 = (z^2 + y_2^2)^{1/2} \tag{9.e\&f}$$

$$y_3 = y - R_p - R_c \qquad r_3 = (z^2 + y_3^3)^{1/2} \tag{9.g\&g}$$

$$y_4 = y - R_p + R_c \qquad r_4 = (z^2 + y_4^2)^{1/2} \tag{9.i\&j}$$

where R_p and R_c are the radii of the particle and collector, respectively; $|\vec{M}_p|$ and $|\vec{M}_c|$ their dipole moments; and r_1 through r_2 the distances separating individual poles on the smaller particle from individual poles on the collector. Here, the z-axis is parallel to flow and the y-axis is parallel to the electric field. In forthcoming discussion this electrical force will be written as

$$\vec{F}_e = \frac{1}{4\pi\varepsilon_o} \frac{|\vec{M}_p|\ |\vec{M}_c|}{R_p R_c} \vec{f}_e \tag{9.k}$$

where $\vec{f}_e$ is the vector describing the line of action of $\vec{F}_e$.

If the particle is much smaller than the collector, the particle's inertia is comparatively small and the collector can be treated as an essentially stationary obstacle about which flow is diverted. Consequently, the collector's center is taken as the origin of the coordinate system.

The smaller particle's trajectory is computed in this coordinate system.

Since no exact solution for the mutual flow fields is known, it is assumed that the presence of the smaller particle does not perturb the collector's flow field. This is true only for infinitesimally small particles (flowline interception), but is also assumed for larger particles from lack of a better alternative. Newton's second law of motion is used to compute the trajectory of the small particle in the electric and flow fields of the collector. Stated vectorially

$$\frac{4}{3}\pi R_p^3 \rho_p \frac{d\vec{S}}{dt} = -6\pi\mu R_p(\vec{S} - \vec{U}) + \frac{1}{4\pi\varepsilon_o} \frac{|\vec{M}_p|\,|\vec{M}_c|}{R_p R_c} \vec{f}_e \tag{10.a}$$

$$\frac{d\vec{r}}{dt} = \vec{s} \tag{10.b}$$

where $\vec{S}$ is the particle velocity, $\vec{U}$ is the fluid velocity around the collector, r is the positional vector, and ρ_p is the particle density. This equation can be nondimensionalized in terms of the following groups and variables

$$\vec{S}^* = \vec{S}/U_\infty \qquad \vec{U}^* = \vec{U}/U_\infty \qquad \vec{fe}^* = 4\vec{fe}\, R_c^{\,2} \tag{11.a,b,c}$$

$$r^* = r/R_c \qquad t^* = \omega t \qquad K_v = \frac{U_\infty}{R_c\omega} \tag{11.d,e,f}$$

$$K_f = \frac{9}{2}\frac{\mu}{R_p^2 \rho_p \omega} \qquad K_e = \frac{3}{4}\frac{\varepsilon_o |\vec{E}|^2}{R_p \rho_p U_\infty \omega} \tag{11.g,h}$$

$$\frac{d\vec{S}^*}{dt^*} = K_f(\vec{U}^* - \vec{S}^*) + K_e \vec{f}_e \qquad \frac{d\vec{r}^*}{dt^*} = K_v \vec{S}^* \tag{11.i,j}$$

It is noteworthy that the equations 11.i and 11.j represent six simultaneous equations whose common solution is uniquely determined by only two constants, the ratios K_f/K_v and K_e/K_v. This can be most easily seen by eliminating time via the chain rule thereby expressing the displacements in the x and y directions as a function of z, the displacement in the direction of flow. Temporal information is not essential for determining the collision cross section.

$$\frac{K_f}{K_v} = \frac{9R_c\mu}{2R_p^{\,2}\rho_p U_\infty} \qquad \frac{K_e}{K_v} = \frac{3\,\varepsilon_o|\vec{E}|^2 R_c}{4R_p\,\rho_p U_\infty^2} \tag{12.a,b}$$

However, in actually solving the equations, all six were carried so as not to obscure velocity information since it can be helpful in judging the validity of results. A fourth order Runge-Kutta routine was used for simultaneous integration of the equations represented by 10.a and 10.b in three dimensions. Parameters input for calculations were K_v, K_f and K_e as specified on the figures.

RESULTS AND CONCLUSIONS

Figure 3 shows the aerodynamic collision cross sections for two induced electric dipoles in the inertial capture regime. Values of K_v, K_f, and K_e used in the trajectory calculations determining these cross sections correspond to two particles of about 20 and 8μ diameters colliding under the influence of gravity and polarized by 0, 30, 70 or 100 kV/m external electric fields. Examples of both parallel and perpendicular orientations of the electric field with respect to particle motion are shown.

By symmetry, parallel orientations all give circular collision cross sections (upper left frame). These cross sections were computed only for comparison with those for perpendicular orientations, since the primary interest of this work lies in the latter case where axisymmetric particle motion cannot be assumed. Trends apparent from these circular cross sections are reasonable. They increase in size with proportionate enhancements of collision efficiencies as the field strength increases from 0 to 100kV/m. However, collision efficiency enhancement per unit increase in the electric field diminishes as 100kV/m is reached.

In the case of perpendicular electric field orientations, aerodynamic collision cross sections become highly noncircular even at 30kV/m and trends in the relative sizes are not as obvious as those for the parallel case. The cross sections elongate in the direction of the poles ($x/R_c=0$) with the formation of lobes and narrow around the equator ($y/R_c=0$). As previously explained, this is due to the two types of forces at play, attractive in the polar regions of the collector and repulsive around the equator. Increasing the field strength to 70kV/m further exaggerates the noncircularity. At 100kV/m, the cross section "fractures" into two separate parts, a lobe above each pole. High electric field strengths result in repulsive forces around the collector's equator sufficient to completely counteract the inertial force of the approaching particle when the distant approach path is near colinear with the z/R_c axis; deflection is such that no collision results.

These interpretations are further substantiated by looking at plotted trajectories for the perpendicular orientation in the $x/R_c=0$ plane (See Figs. 4 and 5). These plots represent only single "slices"

out of the three-dimensional trajectories required to define corresponding cross sections. Since the trajectories in this plane are similar for positive and negative y/R_c, only those for positive y/R_c are drawn. This facilitates placing trajectories for two different field strengths on the same figure so that they can be compared. In all plotted trajectories the innermost concentric circle represents the collector surface; the outermost circle represents a surface of radius R_p+R_c. Trajectories intersecting the outermost surface represent collisions. The most interesting features of these figures are (1) for zero field intensities the 8μ particle crosses streamlines in a very direct manner (inertial capture); (2) with polarization substantial capture occurs on the downstream side of the collector; and (3) at field strengths as high as 100kV/m the repulsion existing between the particles for "dead center" approaches becomes obvious and easily explains the "fracturing" of the cross section into two lobes.

For further contrast, comparable trajectories to those shown in Figures 4 and 5 are shown in Figures 6 and 7 for the parallel orientation of the electric field with respect to the direction of flow. Note that (1) no capture occurs on the downstream side of the collector; (2) the cross section does not form two lobes at 100 kV/m.

Figure 8 is entirely analogous to Figure 3 except that the particle being collected is now only 2μ in diameter rather than 8μ. This combination of particle sizes represents the flowline interception regime. In this instance, even at 70 kV/m the cross section is composed of two lobes in the polar regions of the collector. Increasing the field strength increases the size of the lobes. For this capture regime, the absolute size

of the collision cross sections are much smaller than for the comparable inertial capture cross sections. Large enhancements of the collision efficiency by imposing the external electric field are now apparent for both parallel and perpendicular orientations. Compare the cross section for no electric field (inner most circle of upper left frame) to the lobes for perpendicular orientations (lower frames). Any enhancement for perpendicular orientations and comparable field strengths in the inertial capture regime are more obscure.

The areas of the cross sections discussed in the above paragraphs are translated into numerical collision efficiencies and plotted as a function of electric field strength in Figure 9. At low field strengths the collision efficiencies for flowline interception (R_p/R_c=0.1, 2μ particle) are all much less than comparable collision efficiencies for inertial capture (P_p/R_c=0.4, 8μ particle). For flowline interception, enhancements of the collision efficiency for perpendicular orientations are greater than those for parallel orientations; the opposite trend is observed for inertial capture. In fact, up to 100kV/m virtually no enhancement of the collision efficiency results for the perpendicular orientation. This prediction is based on three-dimensional trajectory calculations and noncircular cross sections. If only two-dimensional trajectories had been used to make these predictions by the method prescribed in the literature, substantially different conclusions would have been drawn (see dotted line); circular cross sections give very optimistic results. Differences in the curvature of these plots compared to those of Semonin (circular cross-sections only) are attributable to the different flow profile and dipole-dipole force models used.

SUMMARY

Determinations of aerodynamic collision cross sections for two induced electric dipoles oriented perpendicular to the direction of particle motion require three-dimensional trajectory calculations. Collision efficiencies derived from two-dimensional trajectories can lead to severe errors.

ACKNOWLEDGMENTS

This work was supported by the Director, Office of Energy Research, Office of Basic Energy Sciences, Materials Sciences Division of the U.S. Department of Energy under contract No. W-7405-ENG-48. The advice and guidance of Dr. R. H. Muller and Professor D. N. Hanson are also gratefully acknowledged.

1. Bird, R. B., Stewart, W. E., Lightfoot, E. N. (1960), Transport Phenomena, Wiley, New York, Chapter 4.

2. Corson, D. R., Lorrain, P. (1962), Introduction to Electromagnetic Fields and Waves, Freeman, San Francisco, London.

3. Davis, M. H., Sartor, J. D. (1967), Nature, 215.

4. Davis, M. H., (1964), Quart. Journ. Mech. and Applied Math., XVII, 499.

5. Farmer, J. C. (1981), LBL-12863, Lawrence Berkeley Laboratory, Berkeley, CA.

6. George, H. F., Poehlein, G. W. (1974), Env. Sci. Tech. 8, 46.

7. Goldshmid, Y., Calvert, S. (1963), AIChE Journal, 352.

8. Jackson, J. D. (1975), Classical Electrodynamics, Wiley, New York, Chapter 4.

9. Knutson, E. O. (1976), Colloid and Interfac. Sci., 54, 453.

10. Kraemer, H. F., Johnston, H. F. (1955), Ind. and Eng. Chem., 47, 2426.

11. Landau, L. D., Lifshitz, E. M. (1959), Fluid Mechanics, Pergamon, London, Chapter VIII.

12. Lindblad, N. R., Semonin, R. G. (1963), J. Geophys. Res., 68, 1051.

13. Michael, D. H., Norey, P. W. (1969), J. Fluid Mech., 37, 565.

14. Mukherjee, S., Nielsen, K. A., Hill, H. C. (1978), Powder and Bulk Solids Tech., 2, 29.

15. Nielsen, K. A., Hill, J. C. (1976), Ind. Eng. Chem. Fundam., 15, 149.

16. Nielsen, K. A., Hill, J. C. (1976), Ind. Eng. Chem. Fundam., 15, 157.

17. Plumlee, H. R., Semonin, R. G. (1965), Tellus, XVII, 356.

18. Sartor, J. D. (1960), J. of Geophy. Res., 65, 1953.

19. Semonin, R. G., Plumlee, H. R. (1966), J. of Geophy. Res., 71, 4271.

20. Shafrir, U., Neiburger, M. (1963), J. of Geophy. Res., 68, 4141.

21. Shaw, D. T., Rajendran, N. (1979), Nuc. Sci. and Eng., 70, 127.

FIGURE CAPTIONS

Fig. 1. Definition of the critical radius used in calculation of circular aerodynamic collision cross sections for $x/R_c = 0$ plane.

Fig. 2. Looking at dipole trajectories in $x/R_c = 0$ plane (2.a) and in $y/R_c = 0$ plane (2.b).

Fig. 3. Aerodynamic collision cross sections for two induced electric dipoles in the inertial capture regime. Values are applicable to two particles, 20μ and 8μ diameters, colliding under the influence of gravity and polarized by external electric fields 0, 30, 70, and 100 kV/m in strength and oriented either parallel (//) or perpendicular (⊥) to the direction of particle motion ($K_f = 2$, $K_v = 11.5$, $K_e = 0$, 1, 5, and 10, respectively).

Fig. 4. Particle trajectories in $x/R_c = 0$ plane for electric field orientations perpendicular to flow. Values correspond to a 20μ collector and 8μ particle colliding under the influence of gravity and polarized by 0 (top half of graph, $K_e = 0$) and 70kV/m (bottom half of graph, $K_e = 5$) electric field strengths. Other parameters used are $K_f = 2$ and $K_v = 11.5$.

Fig. 5. Particle trajectories in $x/R_c = 0$ plane for electric field orientations perpendicular to flow. Values correspond to a 20μ collector and 8μ particle colliding under the influence of gravity and polarized by a 30 (top half of graph, $K_e = 1$) and 100 kV/m (bottom half of graph, $K_e = 10$) electric field strengths. Other parameters used are $K_f = 2$ and $K_v = 11.5$.

Fig. 6. Particle trajectories in $x/R_c = 0$ plane for electric field orientations parallel to flow. Values correspond to a 20μ collector and 8μ particle colliding under the influence of gravity and polarized by 0 (top half of graph, $K_e = 0$) and 70kV/m (bottom half of graph, $K_e = 5$) electric field strengths. Other parameters used are $K_f = 2$ and $K_v = 11.5$.

Fig. 7. Particle trajectories in $x/R_c = 0$ plane for electric field orientations parallel to flow. Values correspond to a 20μ collector and 8μ particle colliding under the influence of gravity and polarized by 30 (top half of graph, $K_e = 1$) and 100kV/m (bottom half of graph, $K_e = 10$) electric field strengths. Other parameters used are $K_f = 2$ and $K_v = 11.5$.

Fig. 8. Aerodynamic collision cross sections for two induced electric dipoles in the flow line interception regime. Values are applicable to two particles, 20μ and 2μ diameters, colliding under the influence of gravity and polarized by external electric fields, 0, 30, 70 and 100 kV/m in strength and oriented either parallel (//) or perpendicular (⊥) to the direction of particle motion ($K_e = 0$, 1, 5, and 10, respectively).

Fig. 9. Collision efficiencies as a function of external electric field strength and orientation for two induced electric dipoles falling under the force of gravity. The magnitude of the error bars are due to the coarse mesh size used in calculations of collision cross sections. Note the dramatic difference in collision efficiencies for $E \perp U_\infty$ for the conventional calculation assuming symmetry and that deduced from three-dimensional trajectories.

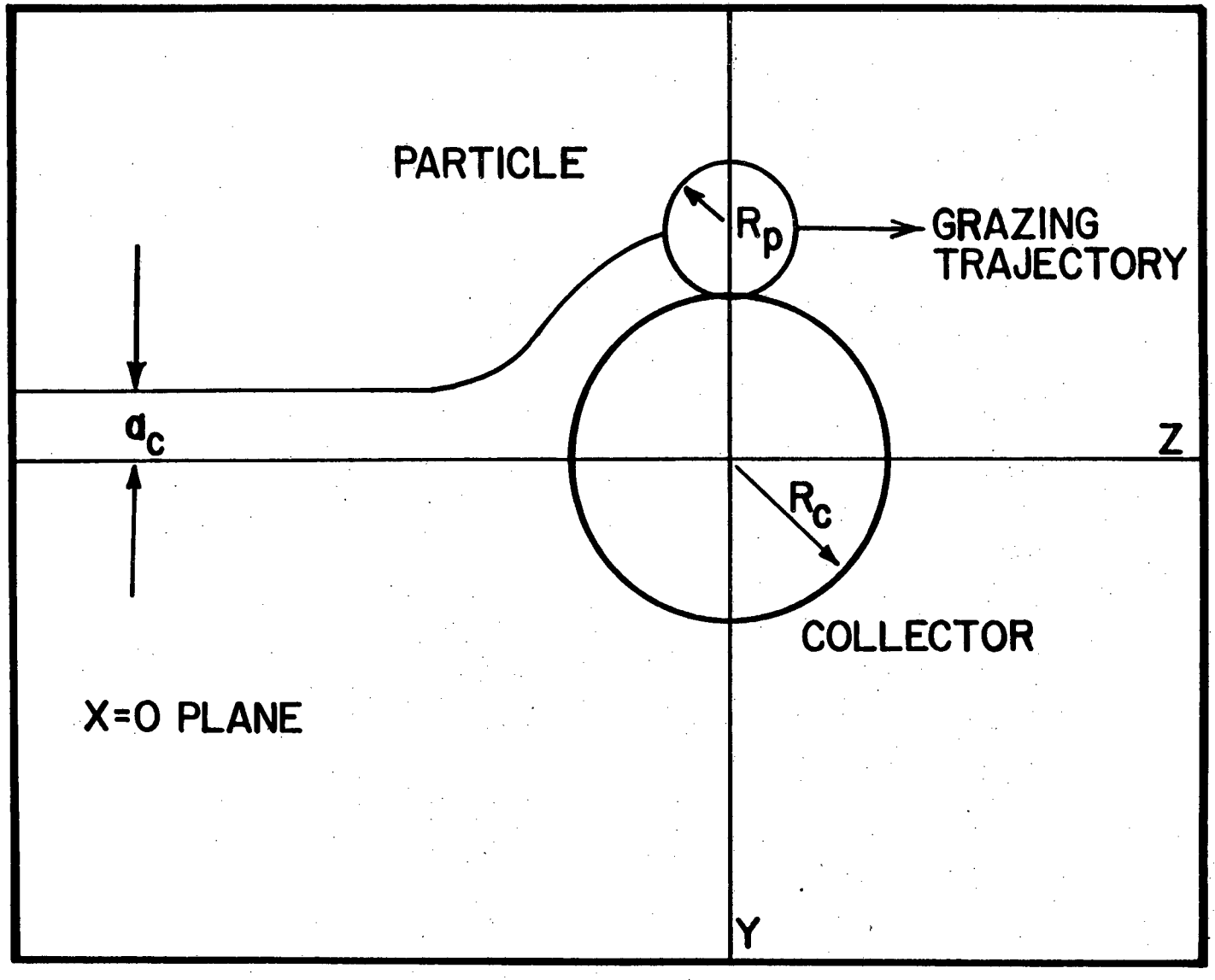

XBL 819-1970

Fig. 1

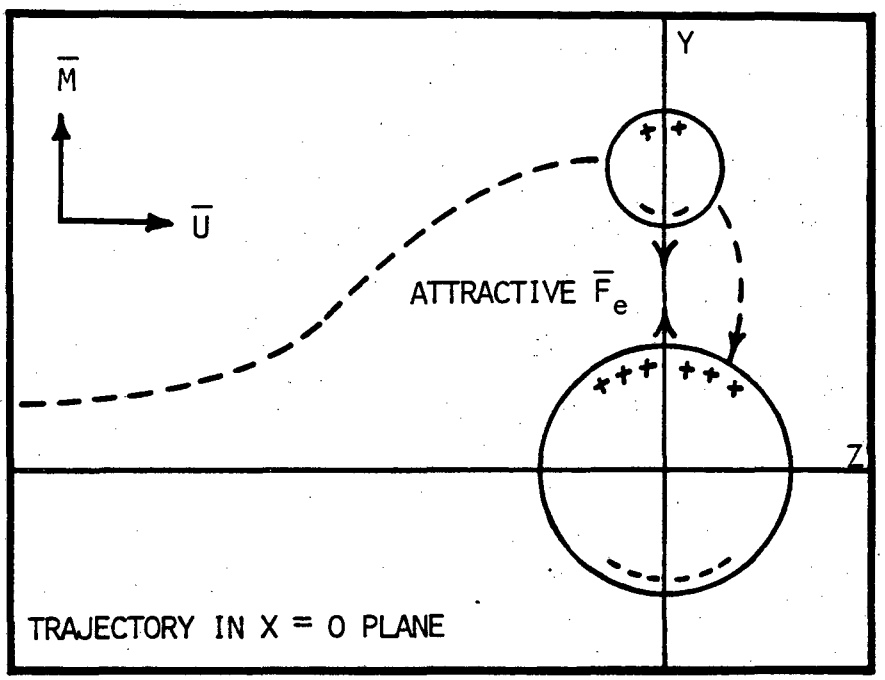

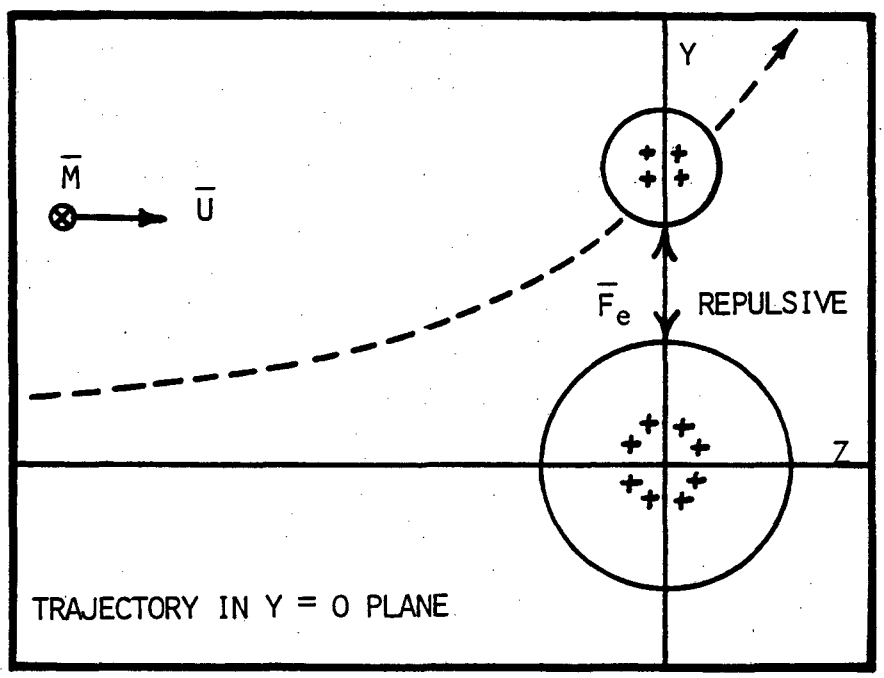

XBL 819-1971

Fig. 2

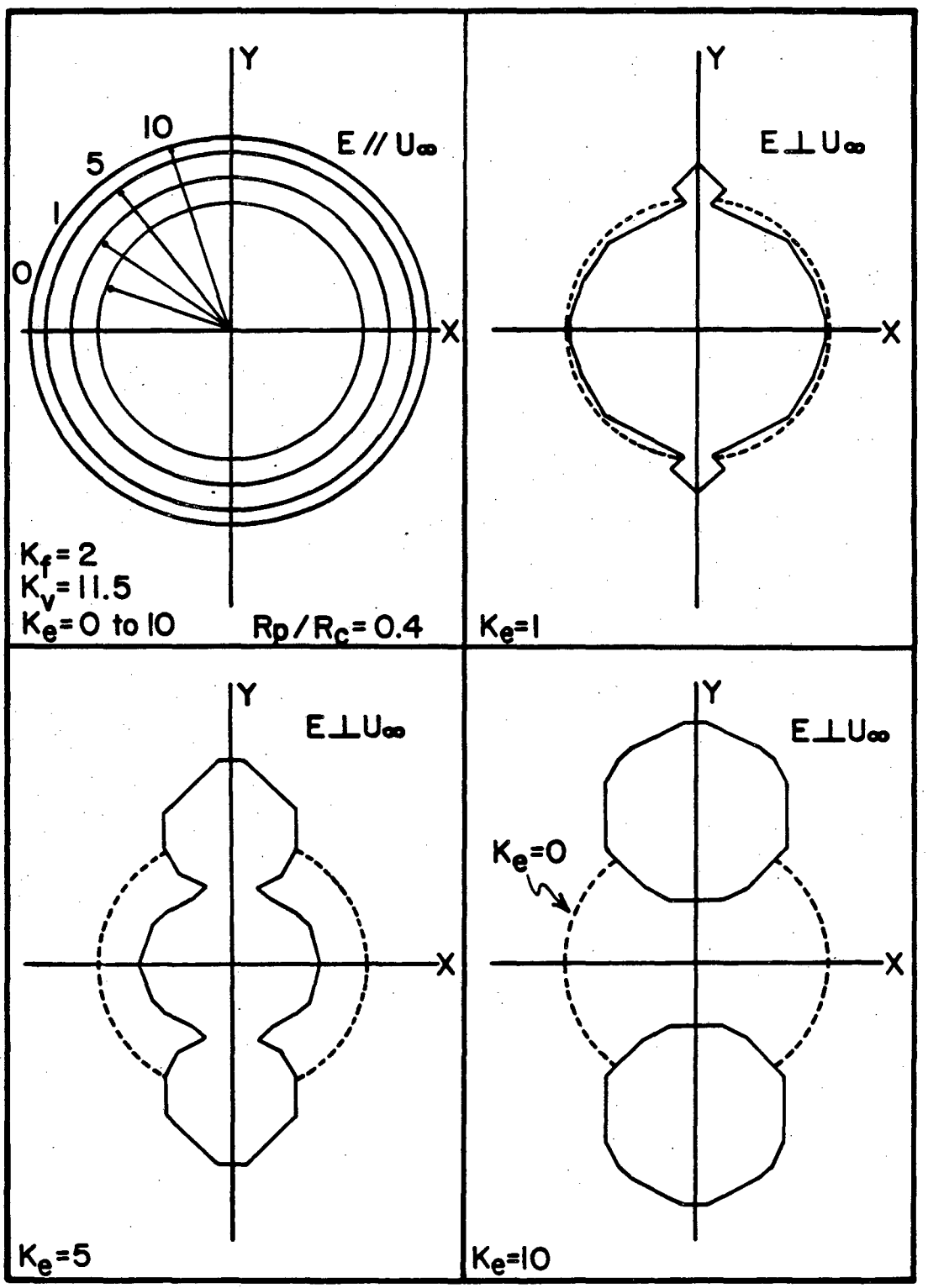

XBL 819-1972

Fig. 3

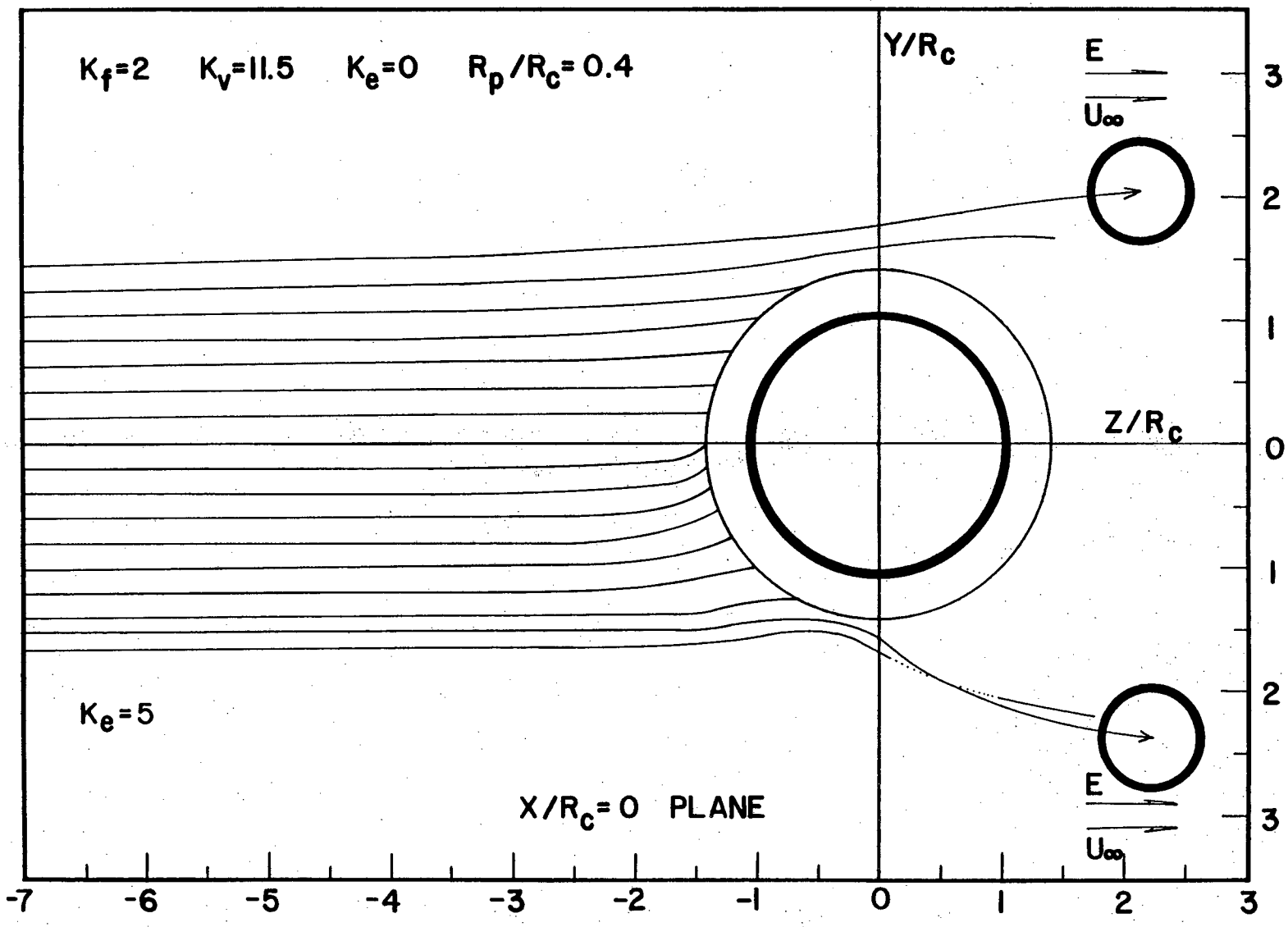

XBL 819-1975

Fig. 4

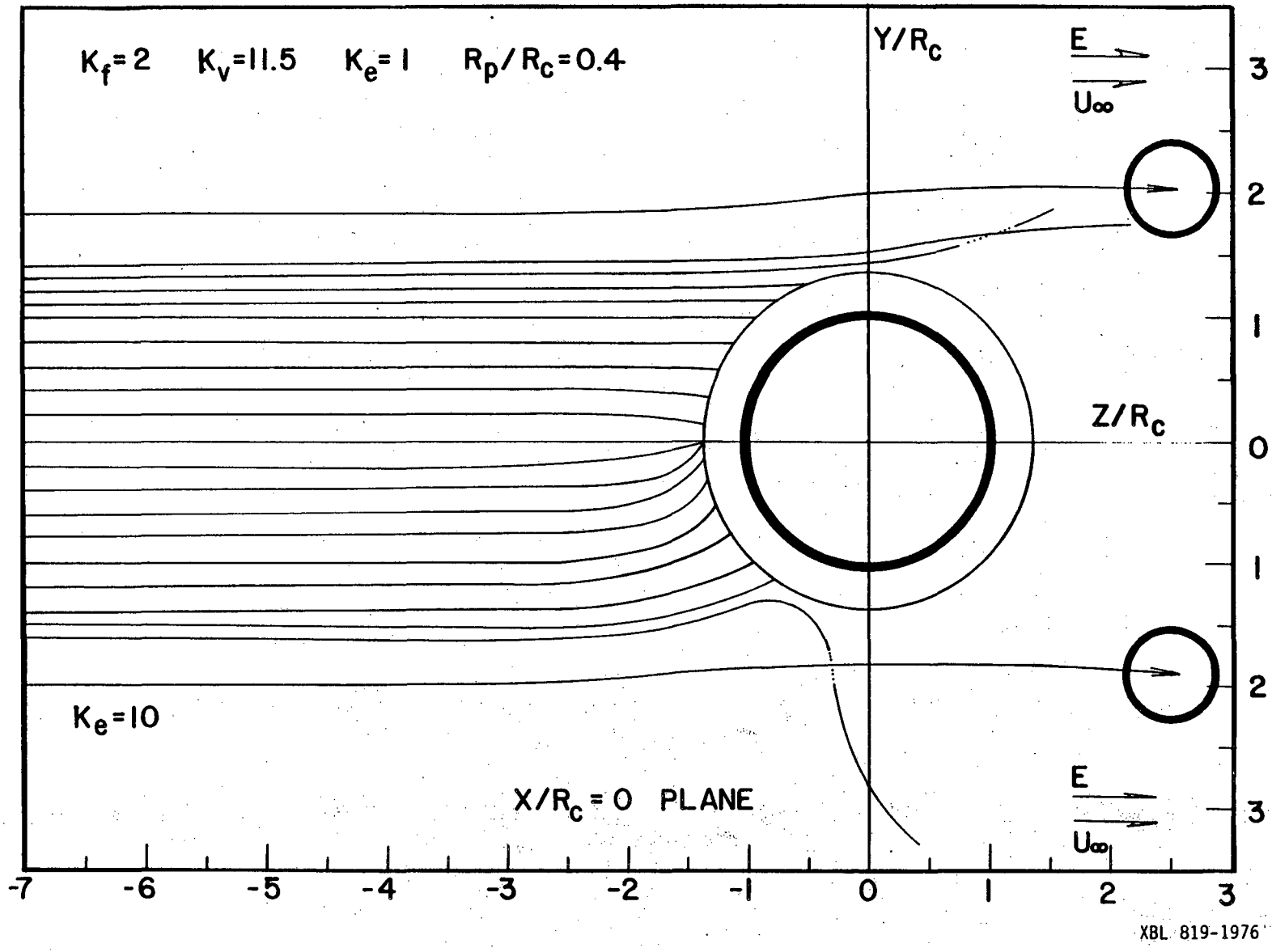
$K_f = 2$ $K_v = 11.5$ $K_e = 1$ $R_p/R_c = 0.4$
$K_e = 10$
$X/R_c = 0$ PLANE
Y/R_c
Z/R_c
E
U_∞
E
U_∞
-7 -6 -5 -4 -3 -2 -1 0 1 2 3
3 2 1 0 1 2 3
XBL 819-1976

Fig. 5

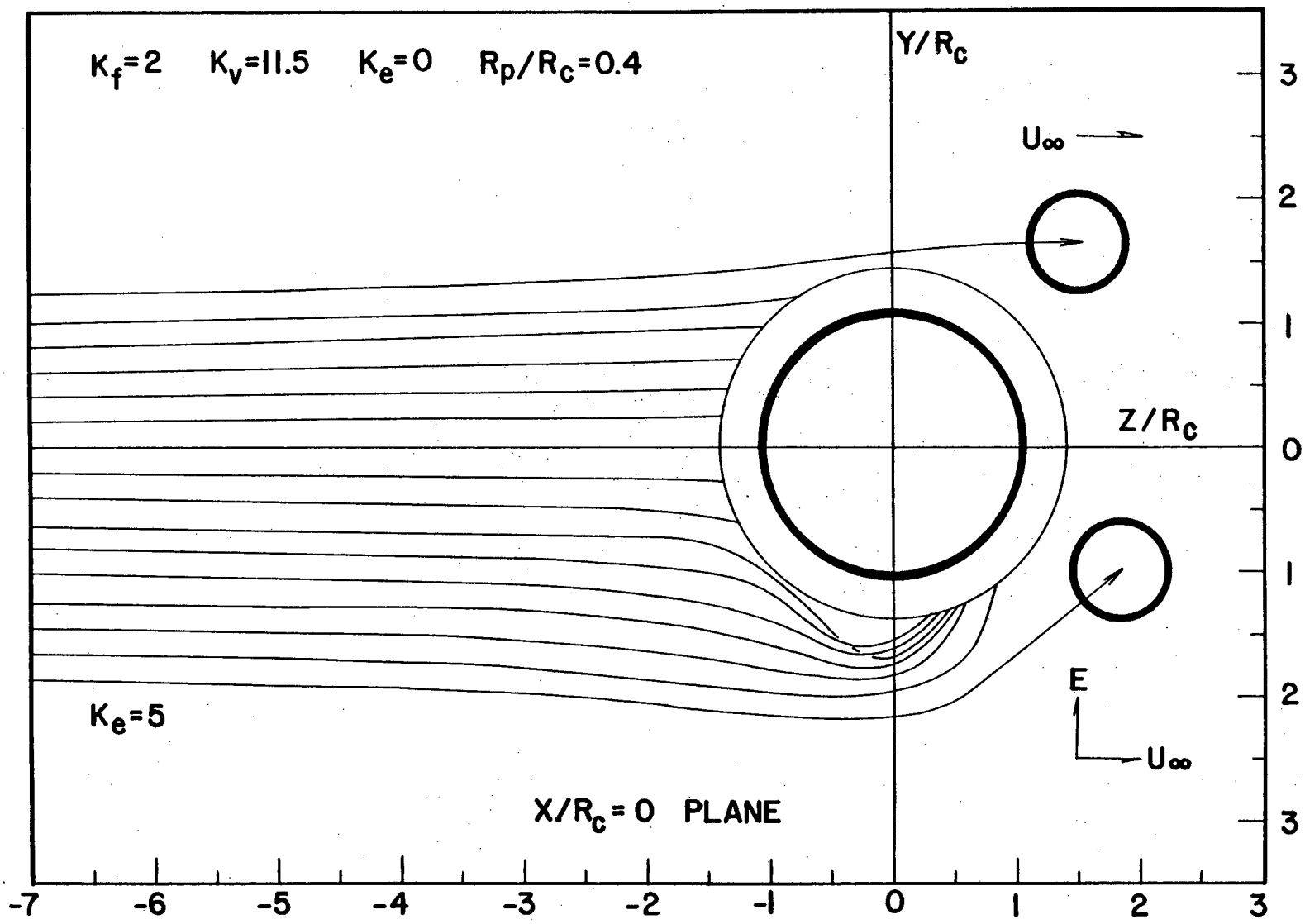

XBL 819-1973

Fig. 6

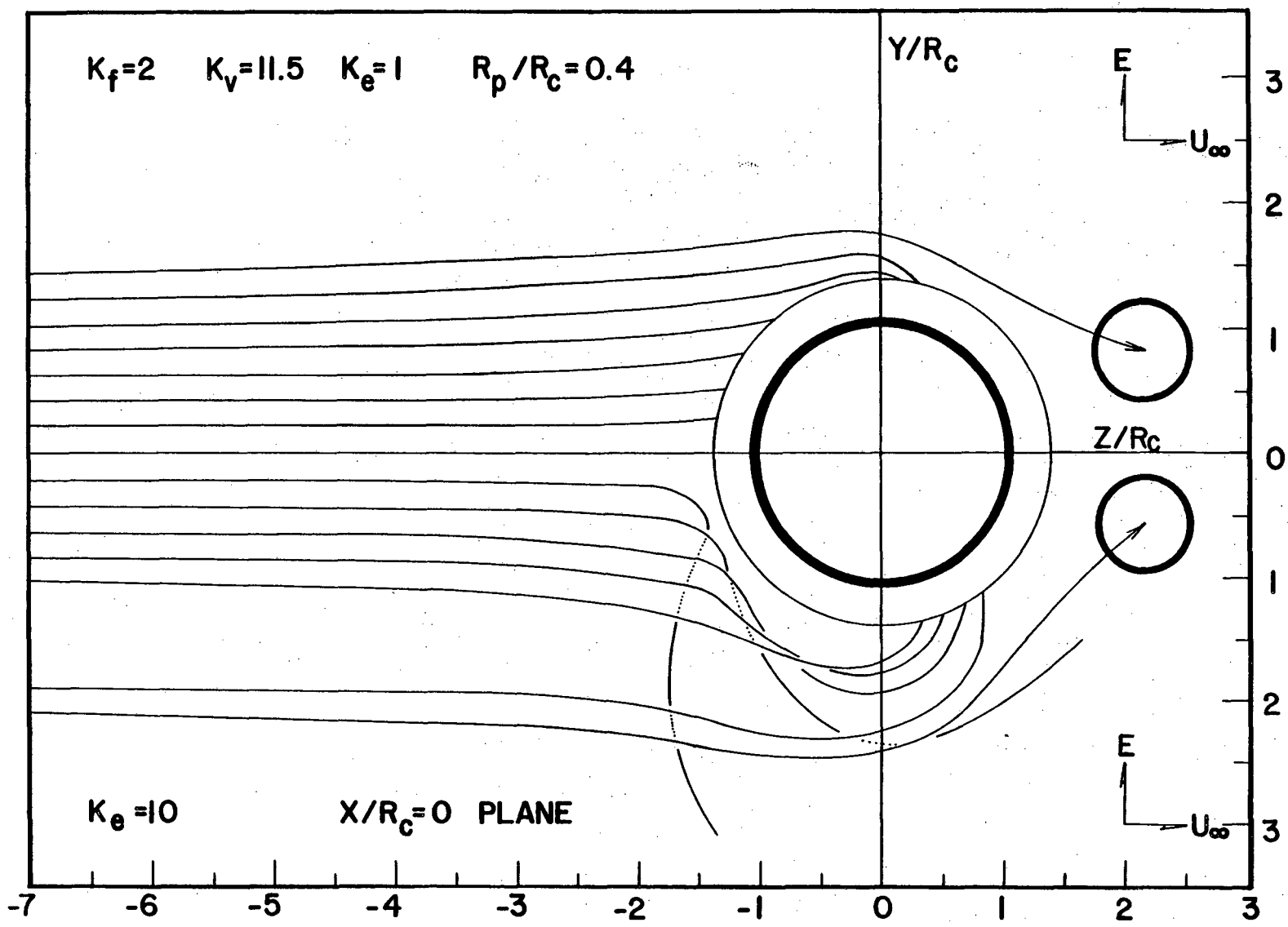

XBL 819-1974

Fig. 7

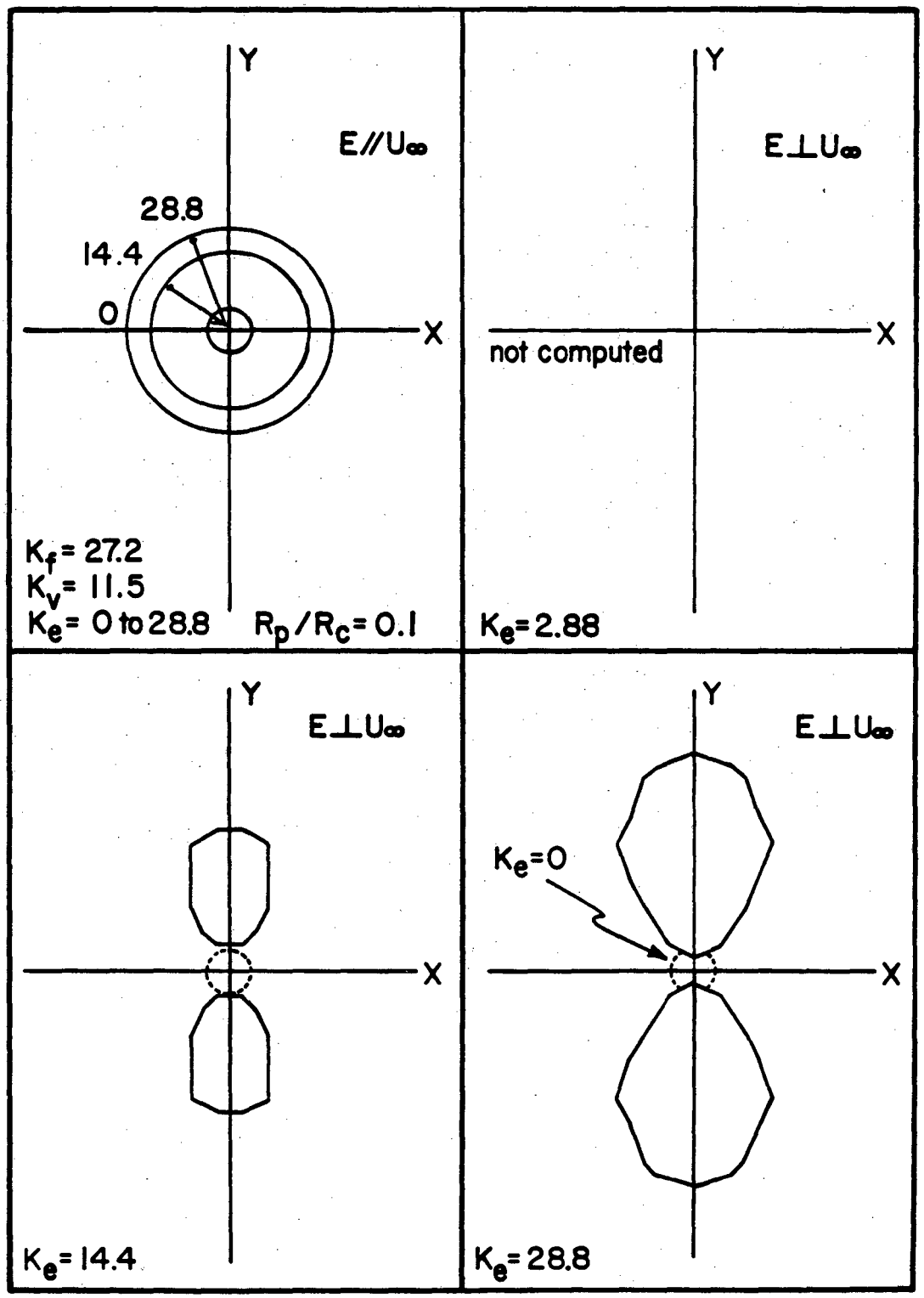

XBL 819-1977

Fig. 8

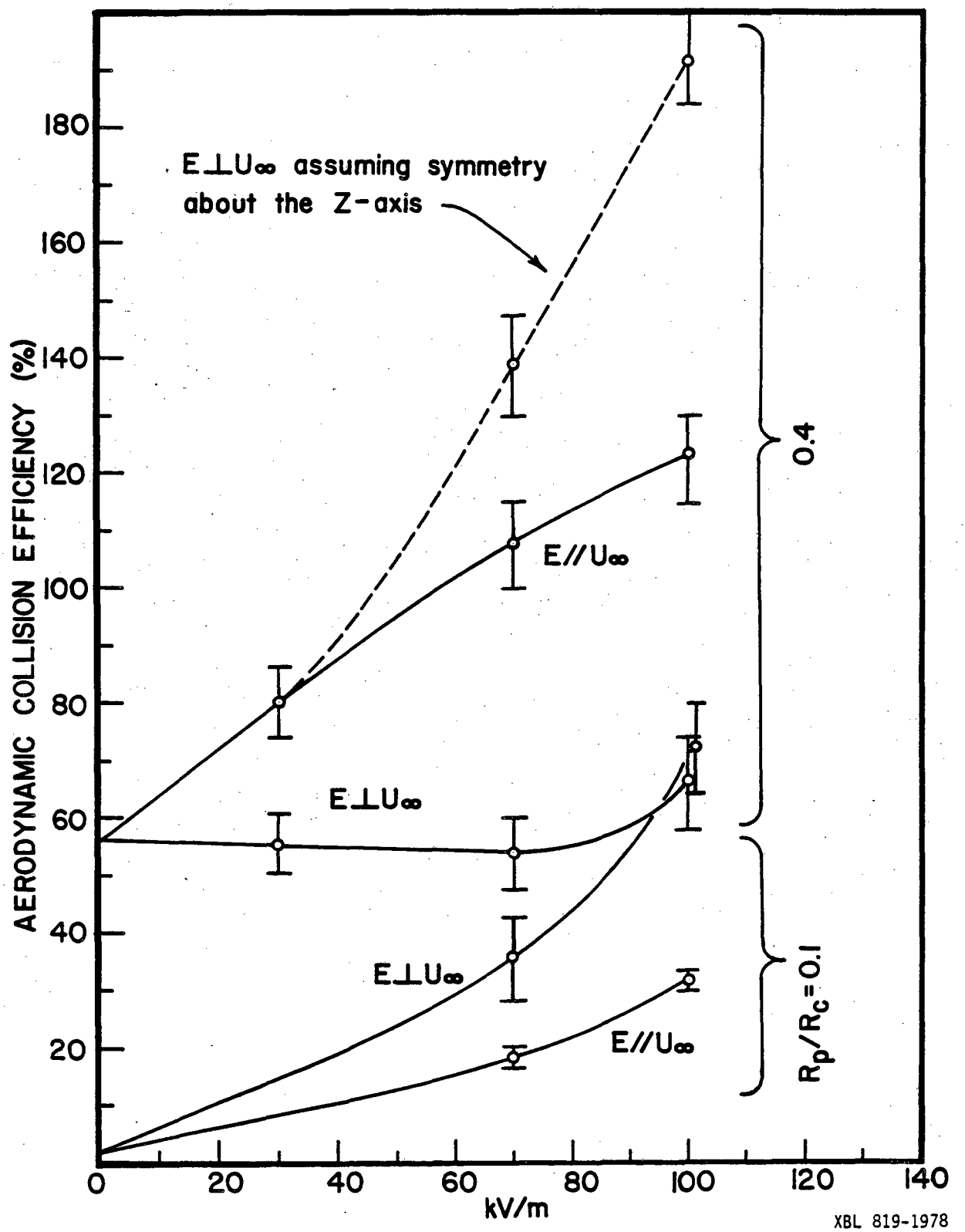
AERODYNAMIC COLLISION EFFICIENCY (%)
180
160
140
120
100
80
60
40
20
0
20
40
60
80
100
120
140
kV/m
E⊥U∞ assuming symmetry about the Z-axis
E//U∞
E⊥U∞
E⊥U∞
E//U∞
0.4
Rp/Rc=0.1
XBL 819-1978

Fig. 9

This report was done with support from the Department of Energy. Any conclusions or opinions expressed in this report represent solely those of the author(s) and not necessarily those of The Regents of the University of California, the Lawrence Berkeley Laboratory or the Department of Energy.

Reference to a company or product name does not imply approval or recommendation of the product by the University of California or the U.S. Department of Energy to the exclusion of others that may be suitable.

TECHNICAL INFORMATION DEPARTMENT
LAWRENCE BERKELEY LABORATORY
UNIVERSITY OF CALIFORNIA
BERKELEY, CALIFORNIA 94720